AIP | Applied Physics Letters

Observation of the high-sensitivity plasmonic dipolar antibonding mode of gold nanoantennas in evanescent waves

Yi-Hsun Chen, Kuo-Ping Chen, Min-Hsiung Shih, and Che-Yuan Chang

Citation: Applied Physics Letters **105**, 031117 (2014); doi: 10.1063/1.4891573
View online: http://dx.doi.org/10.1063/1.4891573
View Table of Contents: http://scitation.aip.org/content/aip/journal/apl/105/3?ver=pdfcov
Published by the AIP Publishing

Observation of the high-sensitivity plasmonic dipolar antibonding mode of gold nanoantennas in evanescent waves

Yi-Hsun Chen,[1] Kuo-Ping Chen,[2,a)] Min-Hsiung Shih,[3] and Che-Yuan Chang[2]
[1]*Institute of Lighting and Energy Photonics, National Chiao-Tung University, No. 301 Gaofa 3rd Rd., Tainan, Taiwan*
[2]*Institute of Imaging and Biomedical Photonics, National Chiao-Tung University, No. 301 Gaofa 3rd Rd., Tainan, Taiwan*
[3]*Research Center of Applied Sciences, Academia Sinica, No. 128 Section 2, Academia Rd., Taipei, Taiwan*

(Received 10 June 2014; accepted 17 July 2014; published online 24 July 2014)

Plasmonic dipolar antibonding modes of gold nanoantennas are observed in evanescent waves. Comparing with the bonding mode for normal incidence, the use of prism coupling to transfer the energy of incident light to plasmonic resonance in nanoantennas not only has a higher extinction coefficient but also achieves higher sensitivity to the surrounding environment. The sensitivity of the antibonding mode of gold nanoantenna is 4.84 times that of the bonding mode in terms of the figure of merit. © *2014 AIP Publishing LLC*. [http://dx.doi.org/10.1063/1.4891573]

Localized surface plasmon resonance (LSPR) has received much attention because of its ability to generate a strong localized electromagnetic field. The oscillation of free electrons at the metal–dielectric interface coupled with an electromagnetic wave can be used in many applications such as bio-detection,[1] fluorescence enhancement,[2] surface enhanced Raman scattering (SERS),[3] metamaterials,[4] and active optoelectronic components.[5] The nanoantenna is one of the most exciting plasmonic nanostructures, because of its enhanced localized electromagnetic field in a small gap[6–8] and its variety of eigenmodes that evolve as a result of mode hybridization.[9,10] Nanoantennas are formed by pairs of metal particles, and the resonance wavelength and intensity of the localized field depend on the structure geometry and refractive index of the surrounding medium.

The plasmonic coupling of nanoantennas can be explained by the plasmon hybridization model introduced by Nordlander *et al.*[11] For symmetric nanoparticle pairs, the coupled mode can be shifted to higher or lower frequencies depending on the phase of the fields generated by the two different dipoles. In the case of p-polarization, the in-phase response is called the bonding mode and the out-of-phase response is called the antibonding mode, in analogy to molecular orbital theory.[11,12] The bonding mode, located at lower energy level, can be strongly excited by normal incidence, but the antibonding mode, located at higher energy level, can hardly be excited by a normal incident plane wave and is not easily observed. In the literature, the antibonding mode has only been excited with highly focused laser beams,[13] the radiation from a local emitter, and the evanescent field produced by total internal reflection (TIR).[9] Although its observation is not easy, the antibonding mode has received much attention because of its slower radiative decay and narrower linewidths.[10,14,15] Lately, a fano resonance in asymmetric nanoantennas has been studied for the sensor application.[16] However, there has been little research for the sensor application of the antibonding modes in symmetric nanoantennas. This work investigates the antibonding mode of gold nanoantennas in an evanescent field and compares the sensitivity to a change in the refractive index of the surrounding medium with that of the bonding mode for normal incidence. Furthermore, in normal incidence, owing to the impedance mismatch between the dielectric and substrate, there is strong reflectance at resonance in the bonding mode that could reduce the coupling efficiency. TIR can be used to minimize the impedance mismatch and transfer the input energy into the antibonding mode of plasmonic resonance and thus achieve higher energy coupling efficiency from incident light to nanoantenna dipole resonance.[17,18]

E-beam lithography is employed to fabricate arrays of gold nanoantennas on a 15 nm indium-tin-oxide (ITO)-coated glass substrate. The design of the nanoantenna arrays is shown in Fig. 1. Comparing with bowtie nanoantennas, square nanoantennas provide a large area of localized field between particles that can be used to sense more molecules bonding with the nanostructure. In addition, there is no need to fabricate sharp tips, which reduces the challenge of fabrication. Scanning electron microscopy shows well-controlled fabrication by e-beam lithography. The square particle x-y dimensions are 97 nm by 98 nm with periodicity of 400 nm in both x and y directions. The thickness of nanoantenna arrays is 35 nm, and the gap between two square nanoparticles is

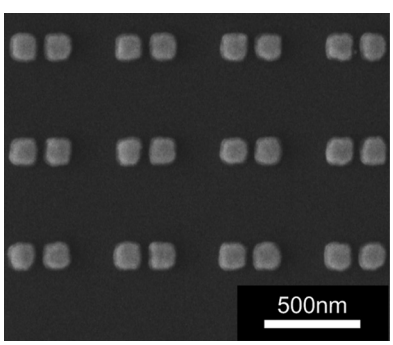

FIG. 1. Scanning electron microscopy image of nanoantenna arrays.

[a)]Email: kpchen@nctu.edu.tw

30 nm. The deviations in nanoantennas dimensions are less than 3%.

Figure 2 compares the far-field spectra in finite element method (FEM) simulation and the experimental result for nanoantenna arrays at wavelengths from 550 to 800 nm. The simulation result fits well with the experimental result. In the simulation, the loss factor of the gold Drude model is 1.4.[19,20] The refractive index of the substrate is 1.52, and the ITO layer is not included in the simulation model. As the surrounding medium is air, normal incidence spectra illuminated by an electromagnetic wave with p-polarization are shown in Fig. 2(a). The resonance wavelength is 675 nm and there are strong localized E-fields in the small gap (see the inset of Fig. 2(a)). Far-field spectra of nanoantenna arrays in prism coupling are shown in Fig. 2(b). Owing to TIR, the transmittance (T) is near zero when the incidence angle is larger than the critical angle. Therefore, the energy of transmitted light can be extracted and transferred to reflectance (R) and extinction (Q_{Ext}) only, which makes Q_{Ext} in Fig. 2(b) twice that in Fig. 2(a).

To investigate the antibonding mode of nanoantenna arrays in an evanescent wave, the nanoantenna arrays are placed on a BK-7 prism (n = 1.52) in both the simulation and experiment. In Fig. 3, nanoantenna arrays are immersed in deionized water (n = 1.33) and illuminated by p-polarized electromagnetic waves from the prism. The figure shows the two-dimensional mapping reflectance spectra with angles of incidence ranging from 0° to 89° and wavelengths ranging from 600 to 880 nm. In the figure, the resonance wavelength of normal incidence is 780 nm when gold nanoantennas are immersed in deionized water. The critical angle of TIR for deionized water and the BK-7 prism is 61.04°. When the incidence angle is larger than the critical angle, the resonance wavelengths are significantly blue shifted from 780 to 680 nm, where the blue shift corresponding well to the higher energy level of the antibonding mode relative to that of the bonding mode.

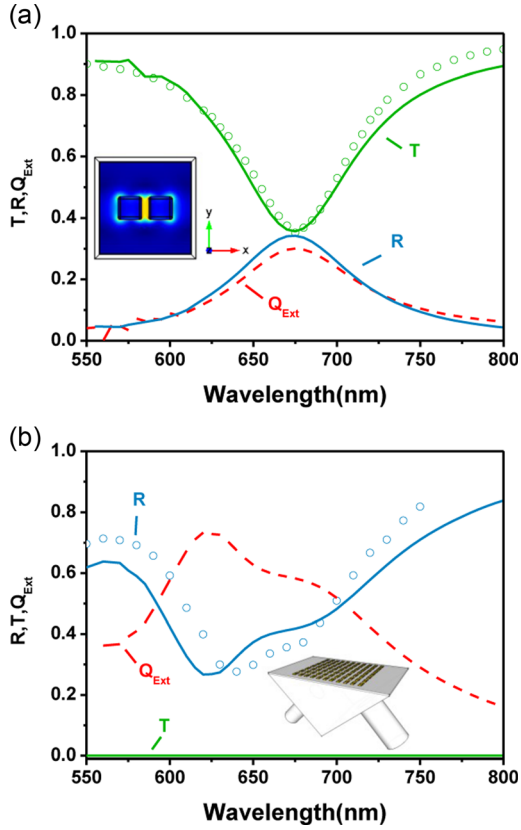

FIG. 2. Far-field spectra of (a) normal incidence and (b) oblique incidence (47°) for p-polarized light. The blue, green, and red curves show the reflectance, transmittance, and extinction, respectively. The solid and dashed lines represent simulation data, and the open circles represent experiment data. The inset of Fig. 2(b) is a schematic of nanoantenna arrays in prism coupling.

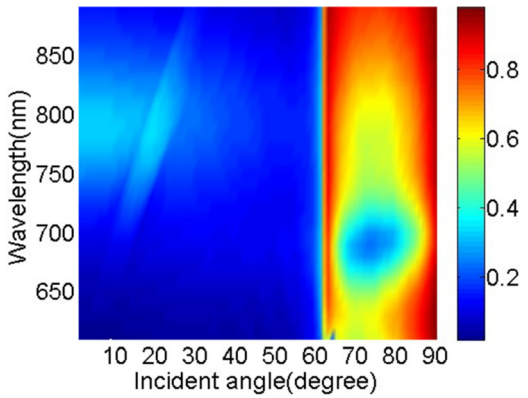

FIG. 3. Two-dimensional mapping reflectance spectra for incidence angles ranging from 0° to 90° and wavelengths ranging from 600 to 880 nm.

The extinction spectra of nanoantenna arrays in prism coupling for different oblique incidence angles are shown in Fig. 4. For normal incidence ($\theta = 0°$), the bonding-mode resonance is excited by p-polarized light at a wavelength of 780 nm. As the angle of incidence increases, the resonance mode at 780 nm becomes weaker; in contrast, the resonance mode at 680 nm becomes stronger. The resonance wavelengths at 780 and 680 nm are independent to the angle of incidence. The resonance mode at 680 nm is dominant when the incidence angle is larger than the critical angle, and is strongest at 72°. Comparison of the resonance modes at $\theta = 0°$ and 72° reveals that an evanescent wave can strongly excite the antibonding mode of gold nanoantennas as predicted in the literature.[9]

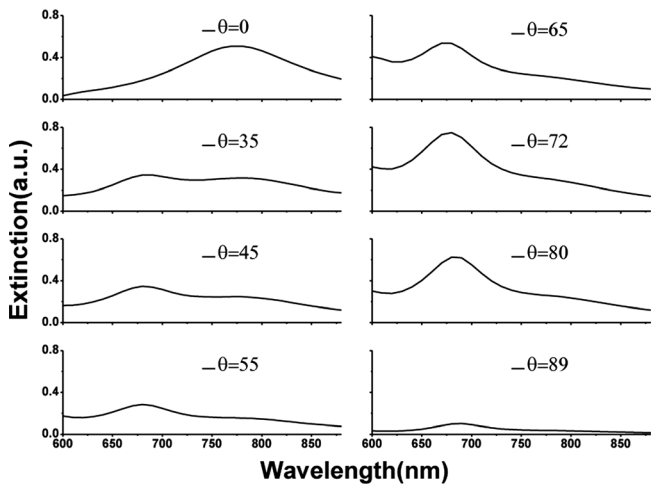

FIG. 4. Extinction spectra of nanoantenna arrays at incidence angles of 0°, 35°, 45°, 55°, 65°, 72°, 80°, and 89°.

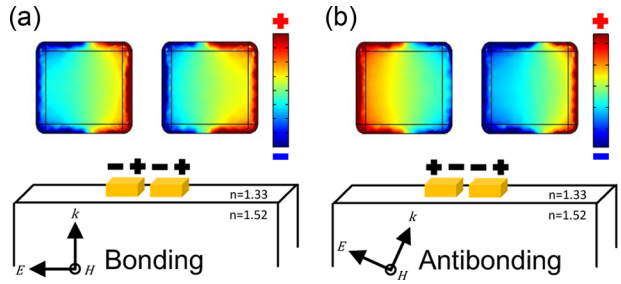

FIG. 5. Charge distribution of gold nanoantennas for (a) normal incidence and $\lambda = 780$ nm and (b) evanescent waves ($\theta = 72°$) at $\lambda = 680$ nm.

The resonance in nanoantennas can be described as the coupling of two individual nanoparticles each with LSPR, which is similar to the bonding and antibonding modes in molecular orbital theory.[10,11] Thus, simulations of charge distributions of nanoantenna arrays for normal incidence and an evanescent wave are carried out, and the results are presented in Fig. 5. In the case of normal incidence, Fig. 5(a) shows the same direction of charge oscillation in two nanorods. Nanoantennas interact strongly and have a strong dipole moment in the so-called "bonding mode." In contrast, the "antibonding mode" occurs at higher energy and has a net zero dipole moment. An evanescent wave generates opposite dipole oscillation in gold nanoantennas and the charge distribution of the antibonding mode is shown in Fig. 5(b).

To better understand the bonding and antibonding modes of nanoantennas arrays, simulated scattering (C_{sc}) and absorption (C_{abs}) cross sections are shown in Fig. 6. Three LSPR coupling conditions are considered: normal incidence and oblique incidence when the angle of incidence is smaller and larger than the critical angle (i.e., incidence angles of 0°, 35°, and 72°, respectively). The bonding mode is observed at 780 nm in both scattering and absorption cross-section spectra for all three angles of incidence. In contrast, the antibonding mode can only be observed at 680 nm in absorption spectra. The absorption cross section of the antibonding mode increases with the angle of incidence. When the angle of incidence is larger than the critical angle, the antibonding mode is clearly observed in absorption spectra but not in scattering spectra. The results provide good evidence that the antibonding mode does not strongly scatter the incident light and the absorption of light is dominant. In addition, in terms of the full width at half maximum (FWHM) of the two resonance modes, the antibonding mode excited by the evanescent wave has narrower linewidth. It is suggested that a nanoantenna chemical sensor in the antibonding mode is more sensitive than a nanoantenna chemical sensor in the bonding mode.

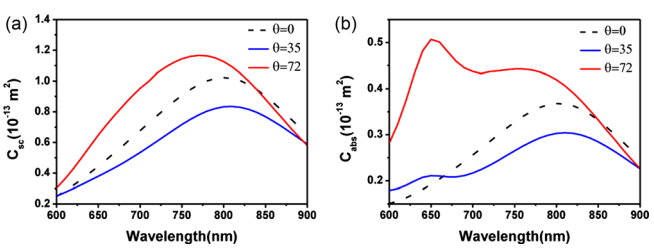

FIG. 6. (a) Scattering and (b) absorption cross section spectra of nanoantenna arrays for incidence angles of 0°, 35°, and 72°.

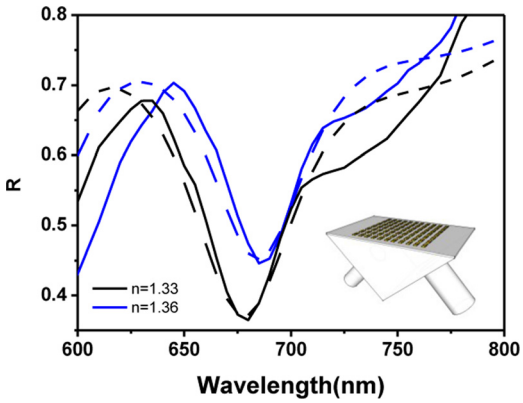

FIG. 7. Simulated (dashed line) and experimental (solid line) reflectance of nanoantenna arrays in prism coupling configuration using water (n = 1.33) and ethanol (n = 1.36) as the surrounding medium.

Reflectance spectra of nanoantenna arrays with a prism coupling configuration measured by angular interrogation instrument are shown in Fig. 7. The sample is illuminated using a white light source (halogen lamp) with grating filters. The reflection of light is collected by a charge-coupled device camera. The polarization of the incident electromagnetic wave is controlled by a linear polarizer. The measurement of the nanoantenna arrays employed a BK-7 prism (n = 1.52), deionized water (n = 1.33) and p-polarized waves. Owing to the limitation of angular interrogation, the reflectance spectra of nanoantenna arrays were measured at 67°. The simulation result fits the experimental result in Fig. 7 well with little deviation. The deviation between simulation and experimental results could be due to the uncertain dimensions of the nanoantenna arrays, imperfect calibration of the SPR instrument, and unexpected error during measurement.

The sensitivity test shown in Fig. 7 is the result obtained with the angular interrogation instrument. The use of 95% ethanol increases the refractive index of the surrounding medium from 1.33 to 1.36, which shifts the resonance wavelength from 675 to 690 nm. $\Delta\lambda/\Delta n$ and the FWHM of nanoantenna arrays in antibonding mode resonance are, respectively, 468 nm/RIU and 49.79 nm. Comparing with normal incidence, $\Delta\lambda/\Delta n$ and FWHM are, respectively, 320 nm/RIU and 165 nm in bonding mode. Furthermore, the figure of merit (FOM) defined as $(\Delta\lambda/\Delta n)$/FWHM is introduced to determine the sensitivity of the chemical nanoantenna sensor. The sensitivity comparison is summarized in Table I. The antibonding resonance mode of gold nanoantennas in evanescent waves has an FOM that is 4.84 times that of the bonding resonance mode in normal incidence.

The antibonding mode of gold nanoantenna arrays in evanescent waves was presented with promised higher sensitivity. Bonding and antibonding resonance modes were

TABLE I. Summary of sensitivity comparison of nanoantenna arrays in prism coupling and normal incidence.

	$\Delta\lambda/\Delta n$ (nm/RIU)	FWHM (nm)	FOM
Prism coupling (67°)	468	49.79	9.4
Normal incidence	320	165	1.94

clearly observed and characterized in both experiment and simulation. The absorption-dominated antibonding mode has higher plasmonic coupling efficiency than the scattering-dominated bonding mode. The antibonding mode of nanoantennas could be observed in both non-normal incident waves and evanescent waves. The antibonding mode excited by evanescent waves has notably higher coupling efficiency and is thus promising in application to an LSPR chemical sensor. In conclusion, the FOM of the antibonding mode in evanescent waves is 4.84 times that of the bonding mode in normal incidence. According to the results of this research, a nanoantenna chemical sensor with higher sensitivity can be designed.

This work was supported by the National Science Council, Taiwan, ROC (Project Nos. 102-2218-E-009-004 and 102-2221-E-009-099). Resources provided by Professor Wei Lee at National Chiao-Tung University, Professor Chii-Wann Lin at National Taiwan University, and Professor Nan-Fu Chiu at National Taipei Normal University are appreciated.

[1]G. V. Naik, J. L. Schroeder, X. Ni, A. V. Kildishev, T. D. Sands, and A. Boltasseva, Opt. Mater. Express **2**, 478 (2012).
[2]A. Kinkhabwala, Z. Yu, S. Fan, Y. Avlasevich, K. Müllen, and W. Moerner, Nat. Photonics **3**, 654 (2009).
[3]N. A. Hatab, C.-H. Hsueh, A. L. Gaddis, S. T. Retterer, J.-H. Li, G. Eres, Z. Zhang, and B. Gu, Nano Lett. **10**, 4952 (2010).
[4]D. Schurig, J. Mock, B. Justice, S. A. Cummer, J. Pendry, A. Starr, and D. Smith, Science **314**, 977 (2006).
[5]M. W. Knight, H. Sobhani, P. Nordlander, and N. J. Halas, Science **332**, 702 (2011).
[6]Z. Liu, A. Boltasseva, R. H. Pedersen, R. Bakker, A. V. Kildishev, V. P. Drachev, and V. M. Shalaev, Metamaterials **2**, 45 (2008).
[7]T. Grosjean, M. Mivelle, F. Baida, G. Burr, and U. Fischer, Nano Lett. **11**, 1009 (2011).
[8]J. Kohoutek, D. Dey, A. Bonakdar, R. Gelfand, A. Sklar, O. G. Memis, and H. Mohseni, Nano Lett. **11**, 3378 (2011).
[9]S.-C. Yang, H. Kobori, C.-L. He, M.-H. Lin, H.-Y. Chen, C. Li, M. Kanehara, T. Teranishi, and S. Gwo, Nano Lett. **10**, 632 (2010).
[10]Y.-C. Chang, S.-M. Wang, H.-C. Chung, C.-B. Tseng, and S.-H. Chang, ACS Nano **6**, 3390 (2012).
[11]E. Prodan, C. Radloff, N. Halas, and P. Nordlander, Science **302**, 419 (2003).
[12]H. Wang, D. W. Brandl, P. Nordlander, and N. J. Halas, Acc. Chem. Res. **40**, 53 (2007).
[13]J.-S. Huang, J. Kern, P. Geisler, P. Weinmann, M. Kamp, A. Forchel, P. Biagioni, and B. Hecht, Nano Lett. **10**, 2105 (2010).
[14]P. Alonso-González, P. Albella, F. Golmar, L. Arzubiaga, F. Casanova, L. E. Hueso, J. Aizpurua, and R. Hillenbrand, Opt. Express **21**, 1270 (2013).
[15]C.-Y. Tsai, S.-P. Lu, J.-W. Lin, and P.-T. Lee, Appl. Phys. Lett. **98**, 153108 (2011).
[16]N. E. Omaghali, V. Tkachenko, A. Andreone, and G. Abbate, Sensors **14**, 272 (2013).
[17]C.-T. Li, H.-f. Chen, I.-W. Un, H.-C. Lee, and T.-J. Yen, Opt. Express **20**, 3250 (2012).
[18]M. Piliarik, H. Šípová, P. Kvasnička, N. Galler, J. R. Krenn, and J. Homola, Opt. Express **20**, 672 (2012).
[19]K.-P. Chen, V. P. Drachev, J. D. Borneman, A. V. Kildishev, and V. M. Shalaev, Nano Lett. **10**, 916 (2010).
[20]V. P. Drachev, U. K. Chettiar, A. V. Kildishev, H.-K. Yuan, W. Cai, and V. M. Shalaev, Opt. Express **16**, 1186 (2008).